OCEANOGRAPHIC CONDITIONS IN THE SOUTHERN BAY OF BENGAL FROM ~0.8 – 1.3Ma

A thesis submitted to the faculty of
San Francisco State University
in partial fulfillment of
the requirements for
the degree

Master of Science

in

Geosciences

by

Alexandria Desirae Lagos

San Francisco, California

January 2019

CERTIFICATION OF APPROVAL

I certify that I have read Oceanographic conditions in the Southern Bay of Bengal from ~0.8 – 1.3Ma by Alexandria Desirae Lagos and in my opinion this work meets the criteria for approving a thesis submitted in partial fulfillment of the requirement for the degree Master of Science in Geosciences at San Francisco State University.

Petra S. Dekens, Ph.D.
Professor

Alexander Stine, Ph.D.
Assistant Professor

Piero Mazzini, Ph.D.
Assistant Professor

OCEANOGRAPHIC CONDITIONS IN THE SOUTHERN BAY OF BENGAL FROM ~0.8 – 1.3Ma

Alexandria Desirae Lagos
San Francisco, California
2019

IODP Expedition 354 drilled an east-west transect of 7 cores in the southern Bay of Bengal that are well situated for better understanding the link between the tropical Indian Ocean and the northern Bay of Bengal. We focus on IODP site U1452 (8°N, 87°E; 3670m water depth), where we reconstructed Mid-Pleistocene (0.84 – 1.27Ma) oceanographic conditions using the Mg/Ca and $\delta^{18}O$ of the planktonic foraminifera, *Globigerinoides Sacculifer*, and the $\delta^{18}O$ and $\delta^{13}C$ of the benthic foraminifera, *Uvigerina peregrina*. We used *G. Sacculifer* Mg/Ca to generate a sea surface temperature (SST) record ranging from 26.9 – 31.2°C during the Mid-Pleistocene. The mean SST remains stable at 28.9°C and has no long-term temperature trend from 0.84 – 1.27Ma. The $\delta^{18}O$ of *G. sacculifer* calcite and SST records were used to estimate the $\delta^{18}O$ of seawater (Bemis et al., 1998), which ranges from 0.7 – 2.2‰. The benthic *U. peregrina* $\delta^{18}O$ record ranges from 3.2 – 4.7‰, which is consistent with LR04 benthic $\delta^{18}O$ stack (3.2 – 4.7‰; Liseicki & Raymo, 2005). While the *U. peregrina* $\delta^{18}O$ record captures the glacial cycles, the timing is offset from the LR04 stack, suggesting further fine-tuning of the IODP site U1452 age model may be needed. The benthic $\delta^{13}C$ record ranges from -1.9 to -0.9‰, with a ~0.3‰ decrease in amplitude through the Mid-Pleistocene, a trend consistent with other deep-ocean $\delta^{13}C$ records.

I certify that the Abstract is a correct representation of the content of this thesis.

12-21-18

Chair, Thesis Committee Date

ACKNOWLEDGEMENTS

I would like to thank and acknowledge my advisor, Dr. Petra Dekens, and my committee members, Dr. Alexander Stine and Dr. Piero Mazzini, for their guidance and contributions to this study. I am indebted to the IODP Expedition 354 team, as this study would not have been possible without their collection and initial processing of the core samples. In addition, I extend my gratitude to the Expedition 354 paleomagnetism team, particularly Dr. Michael Weber and Dr. Brendan Reilly, for their collaboration and contributions related to their work on the site U1452 age model. I would also like to acknowledge the members of the UC Davis Stable Isotope Facility and the UC Santa Cruz Institute of Marine Science's Marine Analytical Laboratory for their assistance, as well as the facilities and instruments utilized for sample analysis. In addition, I would like to thank the John A. and Anna P. Monteverdi Fellowship, COAST, and the Department of Earth & Climate Sciences for their financial support during my time at San Francisco State University. I grateful for my colleagues at SFSU including Theresa Fritz-Endres for her mentorship, Beth Holmes for her encouragement and collaboration, and Drew Lowdermilk for his assistance in the publishing of this thesis. Finally, I would like to thank my family for their tireless support and dedicate this work to my grandfather, Terrell A. Stone, who passed prior to its completion

TABLE OF CONTENTS

List of Tables vi

List of Figures vii

List of Appendices viii

Introduction 1

Method 4

Geochemical Analyses of Foraminifera 5

Results 8

G. sacculifer Sea Surface Temperature 8

G. sacculifer Stable Isotopes 10

U. peregrina Stable Isotopes 11

Discussion 11

Limitations 11

Mid-Pleistocene Sea Surface Temperature 12

Mid-Pleistocene Benthic Conditions 16

Mid-Pleistocene Benthic δ13C 19

Conclusion 21

References 23

Appendices 28

Tables 34

Figures 37

LIST OF TABLES

Table Page

1. Mid-Pleistocene Age Model....................................34
2. Mid-Pleistocene Tropical SST....................................35
3. Mid-Pleistocene Benthic $\delta^{18}O$....................................36

LIST OF FIGURES

Figures Page

1. Bay of Bengal Map 37
2. Bay of Bengal SST Maps 38
3. Age Model 39
4. *G. Sacculifer* Records 40
5. SST Record 41
6. $\delta^{18}O_{sw}$ Record 42
7. Surface Records 43
8. Benthic Records 44
9. A1.1 Expedition 354 Stratigraphic Columns 45
10. A2.1 Contamination Bias 46
11. A2.2 Individual Shell Bias 47
12. A2.3 SST Calibration 48

LIST OF APPENDICES

Appendix Page

1. Bengal Fan Lithology....................26
2. SST Calibration....................28

INTRODUCTION

Sediment cores from the Bay of Bengal in the northern Indian Ocean present a unique opportunity to investigate connections between regional climate, tectonics, and oceanographic processes (Figure 1). The Bay of Bengal and South Asia are characterized by a monsoonal climate, with the majority of the region's annual precipitation delivered as monsoon rainfall during the summer months (Goswami, 2005). In early summer, the heating of Himalayan Plateau creates a land-sea pressure gradient that generates seasonal southwesterly winds (Zhisheng et al., 2015). These winds generate the Southwestern Monsoon Current which transports warm equatorial surface water into the bay (Figure 2; Schott et al., 2009; Zhisheng et al., 2015). The influx of warm water generates critical latent heat for monsoon precipitation and the subsequent rainfall transports sediment from the Himalayan Plateau, through the Ganges-Brahmaputra delta, and into the Bengal Fan (Clift et al., 2008; Jena et al., 2016). The Bengal Fan is comprised of a combination of this terrestrial sediment transported throughout the fan by gravity-driven turbidity currents within the fan's active channels and marine material from the water column (Jena et al., 2016). Recent International Ocean Discovery Program (IODP) expeditions 353 and 354 cored sediments from the Bengal fan to investigate the regional connection between oceanographic conditions, terrestrial processes, and climate recorded in the fan complex.

IODP expedition's 353 and 354 are part of an integrated effort to utilize marine sediment cores to better understand the Cenozoic evolution of regional oceanographic conditions, monsoon climate, and the uplift and erosion of the Himalayan Plateau

(France-lanord et al., 2015). Due to a scarcity of paleoceanographic records in the Indian Ocean, there is a limited understanding beyond modern observations of how these regional processes interact and evolve over-time. The east-west transect of 7 cores Expedition 354 collected in the southern Bengal Fan (8°N) provide an opportunity to reconstruct conditions between the tropical Indian Ocean and northern monsoon system (Figure 1; Clemens et al., 2015; France-Lanord et al., 2015). Expedition 354's transect lies in the path of the Southwest Monsoon current (Figure 2), which connects the equatorial Indian Ocean to the monsoon system vis the seasonal transport of warm equatorial surface water north, towards the Expedition 353 sites (Clemens et al., 2015; Schott et al., 2009; Zhisheng et al., 2015). Together, Expedition 353 and 354 can be used to evaluate oceanographic and monsoon dynamics in the Bay of Bengal through time. This study focuses on oceanographic conditions at IODP 354 site U1452 (8°N, 87°E; ~3670m depth), which contains a well-preserved hemipelagic layer spanning the Mid-Pleistocene.

At all Exp. 354 sites, a well-preserved, regionally extensive hemipelagic layer was targeted for paleoceanographic study as frequent turbidity currents often cause unconformities making it difficult to generate continuous records (Appendix 1; Figure A1.1; France-Lanord et al., 2016b). Due to the turbidity-driven deposition in the fan, it was uncertain whether it was possible to generate paleoceanographic records with the core sediments. However, the onset of the Mid-Pleistocene is characterized by a decrease or possible cessation of turbidite deposition near the 354 transect, leading to the excellent preservation of this interval at all 7 sites (Figure A1.1; France-Lanord et al., 2016b;

Weber & Reilly, 2018). The preliminary ship-board age model composed of magnetic reversals, sediment lightness (L*), and the Oldest Toba Tephra suggested the hemipelagic interval included the Mid-Pleistocene from ~0.8 – 1.2Ma (France-Lanord et al., 2016; Weber & Reilly, 2018).While all sites contain the Jaramillo magnetic reversal, site U1452 was selected for this study because the initial shipboard age model identified five magnetic reversals including the Bruhnes, Matuyama, Jaramillo, and Cobb Mountain subchrons (Table 1; Figure 3; Weber & Reilly, 2018). As U1452 has best age control of the 7 sites, the L* records from the other hemipelagic intervals have been correlated to the updated U1452 (Weber & Reilly, 2018). Therefore, any error within the U1452 age model affects age models at all sites. The refinement of these age models is critical, as comparing changes in sedimentation rate laterally across the fan will contribute to Exp. 354's understanding of fan evolution (France-Lanord et al., 2016b). An objective of this study is to evaluate the accuracy of the U1452 age model by creating foraminifera oxygen isotope ($\delta^{18}O$) records for the Mid-Pleistocene interval to compare to a global $\delta^{18}O$ stack.

At IODP site U1452, this hemipelagic interval is found in core 37F (184.7 – 189.4mbsf) and the post-cruise refinement of the age-model determined the interval does include the Mid-Pleistocene from ~0.84-1.27Ma (Table 1; Figure 3; Weber & Reilly, 2018). (Weber & Reilly, 2018). This time interval is referred to as the Mid-Pleistocene Transition (MPT, ~0.8-1.2Ma); a crucial period in which the Earth's ice sheets began responding to changes in eccentricity (100kyr cycles) rather than obliquity (41kyr cycles), as it had prior to 1.2Ma (Huybers, 2007; Lisiecki & Raymo, 2007; Raymo et al., 2006). The shift from 41kyr to 100kyr frequency has been well documented in the LR04 global stack of benthic foraminifera $\delta^{18}O$ records (Lisiecki & Raymo, 2005). However, benthic foraminifera record the $\delta^{18}O$ signature of deep water, representative of high latitude climate, and do not provide information about the low latitudes (Herbert et al., 2010; Huybers, 2006; Lisiecki & Raymo, 2007). The Indian Ocean's response to the MPT is particularly uncertain since records in the basin are scarce. While the cause of the MPT shift in glacial frequency is debated, its effects can be observed in a variety of climate records (Huybers, 2006; Medina-Elizalde & Lea, 2005; Raymo et al., 1997; Raymo et al., 2006). The hemipelagic layer at site U1452 presents an opportunity to use the geochemistry of preserved foraminifera calcite to reconstruct surface and deep-ocean conditions to better understand how the tropical Indian Ocean was affected by the MPT.

METHODS

IODP site U1452B was drilled to a depth of 217.7m. Core 37F (184.7-189.4 mbsf) is hemipelagic and consist of calcareous, microfossil rich clays with grain sizes between 0.15 and 0.25mm (France-Lanord et al., 2016). The working half of 37F was sampled every 2cm, with the goal of creating ~1-2 kyr resolution records for this time period. The samples were disaggregated in deionized water before filtering through 63µm sieve. Sediments >63µm were collected on filter paper and oven dried at 45°C to prepare for picking. The dry sediments were sieved into two size fractions, 250-355µm and 355-425µm. Each size fraction was examined under a microscope and shells of *Globeriginoides sacculifer* and *Uvigerina peregrina* were picked for analysis. *G.*

sacculifer is a planktonic species that spends its juvenile life stage in the photic zone of the surface mixed layer due to the presence of symbiotic dinoflagellates (Bé et al., 1982). The adult stage of the *G. sacculifer* life cycle is easily identifiable by the growth of a final, sac-like shell chamber, indicating the organism has migrated deeper in the water column and grown gametogenic calcite that alters the shell chemistry (Bé et al., 1982; Brummer et al., 1986). *G. sacculifer's* ontogenetic morphology allows us to preferentially pick the juvenile shells commonly used as a proxy for surface conditions (Brummer et al., 1986). In comparison, *U. peregrina* are an infaunal, benthic species that spends its entire life cycle in the first 1-2cm of sediment (Wells et al., 1994). As a result, they are a commonly used benthic proxy due to their continuous exposure to sediment pore-water in equilibrium with bottom-water chemistry (N J Shackleton, 1974).

Geochemical Analyses of Foraminifera

Approximately 20-30 *G. sacculifer* shells were selected and weighed on a Sartorius CPA2P balance with a precision of 0.001mg. The shells were gently cracked open between glass plates while observing through a microscope to ensure samples were not crushed. The shell fragments were mixed with a paintbrush to homogenize the sample prior to being split for Mg/Ca and $\delta^{18}O$ analyses. Measuring $\delta^{18}O$ and Mg/Ca on splits of well-mixed material reduces bias caused by differences in individual shell chemistry. When the sample size was large enough, it was divided into two splits of Mg/Ca (~250-600µg each) and one $\delta^{18}O$ (~20-90µg). For the benthic $\delta^{18}O$ samples, five *U. peregrina* shells were selected, which yielded approximately 150-250µg per sample.

For $\delta^{18}O$ analysis *G. sacculifer* and *U. peregrina* shells were covered with ultra-pure deionized water and ultra-sonicated for 5 seconds before excess water was carefully siphoned away. The same process, without sonication, was performed with methanol and the samples were left uncapped in a laminar flow bench to dry. The samples were vacuum roasted at 75°C to remove moisture before analysis using a GVI Optima Stable Isotope Ratio Mass Spectrometer (SIRMS) at the University of California, Davis, Isotope facility. The UCD-SM92 standard was processed for $\delta^{18}O$ (σ = 0.058‰) and $\delta^{13}C$ (σ = 0.029‰) every 7 samples.

The Mg/Ca cleaning process includes a set of initial rinses, reductive and oxidative steps, and weak acid leaches to remove contaminants following standard trace metal cleaning methods established by Boyle & Keigwin (1985). Samples cleaned using this rigorous trace metal method consistently show a reduction in Mg/Ca values, which reduces uncertainty due to magnesium contamination (Barker et al., 2003; Boyle & Keigwin, 1985; Elderfield et al., 2006).

The samples were initially rinsed three times with ultra-pure deionized water, twice with methanol, and a final three times with ultra-pure water, including 30 seconds of ultra-sonication with each rinse. These rinses remove clays that can contain between 1-10% contaminant Mg by weight (Barker et al., 2003). In the reductive step, 100µl of a solution of 10ml ammonium citrate, 10ml ammonium hydroxide, and 1ml 85% anhydrous aqueous hydrazine was added to each sample. The samples were securely closed to prevent outgassing and placed in a hot water bath for 30 minutes with ultra-sonication for 5 seconds every 2 minutes. The reductive solution was removed with 3 ultra-pure water rinses (with 30 second ultra-sonication between each) before proceeding to the oxidation step. The oxidation step removed organic material (Barker et al., 2003) using a solution of 50µl 30% hydrogen peroxide and 30ml of 0.1N sodium hydroxide. After adding 250µl of the solution to each sample, the caps were closed and set in a hot water bath for 10 minutes and ultra-sonicated for 5 seconds at 5 and 10 minutes. Next, the oxidative solution was removed with an ultra-pure dejonized water rinse without the ultra-sonication followed by a 5-minute hot water bath and a second rinse. The samples were then covered with ultra-pure deionized water and transferred to larger, acid-leached vials using a 100µl pipette that was rinsed every sample. Finally, the samples were leached with weak acid to remove any absorbed contaminants remaining (Martin & Lea, 2002). Using a 100µl pipette, 0.001N, nitric acid was added to each row of 10 samples, then diluted with ultra-pure deionized water to prevent over-dissolution of shell calcite. The diluted acid was siphoned off, and the remaining acid was removed with 2 rinses with ultra-pure deionized water.

The Mg/Ca of the cleaned samples was measured on an Inductively Coupled Plasma Optical Emission Spectrometer (ICP-OES) at the University of California, Santa Cruz. Two foraminifera standards composed of *G. sacculifer* and *Globeriginoides crassiformis* were cleaned and analyzed every 28 samples to evaluate consistency in cleaning methodology. The *G. sacculifer* standard had a standard deviation of 0.11 mmol/mol and a variance of 0.012 mmol/mol. The *G. crassiformis* standard had a standard deviation of 0.21 mmol/mol and a variance of 0.043 mmol/mol. Additionally, a foraminifera liquid standard, FLCS-2, was analyzed every 10 samples to monitor instrument error. The

FLCS-2 standard from all ICP-OES runs yielded a standard deviation of 0.025 mmol/mol and variance of 0.00064 mmol/mol.

RESULTS

G. sacculifer Sea Surface Temperature

We reconstructed SST during the Mid-Pleistocene using the Mg/Ca ratio of *G. sacculifer* shell calcite. *G. sacculifer* Mg/Ca ranges from 2.91 to 4.18 mmol/mol (Figure 4). The Mg/Ca record has a relatively consistent mean of 3.52 mmol/mol throughout the record and does show any long-term trends (Figure 4). A concern when using shell calcite Mg/Ca as a proxy is magnesium contamination from clays, organics, metal oxides, and laboratory materials that can lead to higher Mg/Ca values (Appendix 2; Barker et al., 2003). The *G. sacculifer* Mn/Ca ratio was also measured to test for magnesium contamination (Appendix 2), as common contaminants are also high in manganese. The Mn/Ca ranges from 0.0001 to 0.76 mmol/mol, which is within the typical range for oxidative-reductive cleaning methodology and does not indicate contamination (Pena et al., 2005). Another concern was bias in the Mg/Ca record from individual shell characteristics, such as shell mass, due to poor sample homogenization. Therefore, we created a scatterplot of Mn/Ca vs. Mg/Ca values, as any correlation would suggest contamination during cleaning or analysis (Figure A2.1). A second scatterplot was made to observe any potential correlation between average foraminifera shell mass and Mg/Ca (Figure A2.2). A trendline was a fitted to each scatterplot, and the low R^2 values of 0.008 for Mn/Ca and 0.06 for average foraminifera shell mass does not indicate a correlation with Mg/Ca (Figure A2.1, A2.2). This indicates the bulk Mg/Ca samples used were not biased by contamination or individual shell characteristics and can be used to estimate SST (Figure A2.1, A2.2).

Multiple calibration equations were tested to convert Mg/Ca to SST (Appendix 2). The standard calibration converts Mg/Ca based on the positive, exponential relationship between Mg/Ca concentration and water temperature as well as constants adjusted by foraminifera species, in this case *G. sacculifer* (Anand et al., 2003). However, site U1452 located at ~3670m water depth and this calibration does not account for the preferential dissolution of magnesium rich portions of calcite shells (Rosenthal et al., 2000). Dissolution lowers Mg/Ca values in shell calcite and can occur post-burial and in the water column, more prominently at deep-ocean sites like U1452 (Dekens et al., 2002). Without correcting for dissolution, the standard equation underestimates average SST at 24.7°C, far lower than the modern SST average of ~29°C (Figure A2.3; Anand et al., 2003; Levitus, 1982). Therefore, we tested two additional calibrations that correct for the effects of dissolution based on depth and deep-water carbonate ion (ΔCO_3^{2-}) saturation (Dekens et al., 2002). The depth and ΔCO_3^{2-} dissolution calibrations resulted in very similar SST records with average temperatures of 28.3°C and 28.9°C, respectively (Figure A2.3). However, the depth equation is corrected to either the Pacific or Atlantic basins and site U1452 is located in the Indian Ocean (Appendix 2). Therefore, the *G. sacculifer* Mg/Ca record was calibrated to temperature in degrees Celsius using the carbonate ion (ΔCO_3^{2-}) dissolution corrected formula below (Dekens et al., 2002; Appendix 2; Figure 5).

$$SST = [\ln((Mg/Ca)/(0.31))/(0.084)] - (0.048 * \Delta CO_3^{2-}) \qquad \Delta CO_3^{2-} = 0.24$$

The resulting SST record ranges from 26.9 to 31.2°C, which is similar to modern SST (29 ± 0.8°C average) (Levitus, 1982). There is no long-term trend in SST from 0.84 – 1.27Ma, but the record does demonstrate a cyclicity similar to glacial-interglacial cycles (Figure 6). The record's mean is 28.9°C with a variance of 0.69. The SST amplitude at site U1452 remained consistent at ~1.3°C throughout the MPT, except for an increase to ~1.7°C from 1.095 – 1.089Ma (Figure 6). However, there is the possibility of error in the estimation of amplitude due to gaps in the record near SST peaks caused by low foraminifera abundance.

G. Sacculifer Stable Isotopes

G. sacculifer $\delta^{18}O_{CaCO3}$ values range from -2.45 to -0.71‰. The $\delta^{18}O_{CaCO3}$ mean is -1.15‰ with a variance of 0.095 (Figure 4). The *G. sacculifer* $\delta^{13}C$ record ranges from 0.64 to 2.4‰ with a mean of 1.47‰ and variance of 0.079. The $\delta^{18}O_{CaCO3}$ values were converted to $\delta^{18}O$ of seawater ($\delta^{18}O_{SW}$) using the paired Mg/Ca SST values to remove the effect of calcification temperature (Figure 7; Shackleton et al. 1974). The $\delta^{18}O_{SW}$ record varies between 3.39 and -0.07‰ and was calculated using the equation below (Bemis et al., 1998).

$$\delta^{18}O_{SW} =((-4.38) + SQRT((19.1844) - (6.76) - ((0.4)*(SST)))/(0.2)) - (\delta^{18}O_{CaCO3})$$

U. peregrina Stable Isotopes

The site U1452 *U. peregrina* $\delta^{18}O$ ranges from 3.2 to 4.7‰, with a mean of 3.98‰ and a variance of 0.1. The record is consistent with LR04 benthic $\delta^{18}O$ record (3.2 to 4.7‰) and contains similar glacial-interglacial cycles (Lisiecki & Raymo, 2005, Figure 8). However, the timing of the glacial cycles is different between the two records, with features being offset as much as ~20kyr. Additionally, the record decreases in amplitude by ~0.4‰ across the MPT (Figure 8).

The *U. peregrina* $\delta^{13}C$ record ranges from -1.9 to -0.9‰ and has a mean of -1.38‰ and variance of 0.061 (Figure 8). The site U1452 benthic $\delta^{13}C$ record exhibits a gradual decrease $\delta^{13}C$ over the Mid-Pleistocene (Figure 8). As a result, the $\delta^{13}C$ amplitude also decreases by ~ 0.3‰ during the Mid-Pleistocene.

DISCUSSION

Site U1452 Limitations

This study aimed to determine if oceanographic conditions could be reconstructed in a complex alluvial fan environment and whether the tropical Bay of Bengal was being influenced by the MPT. While foraminifera were preserved in site U1452's hemipelagic interval, there were some obvious limitations to generating paleoceanographic records in an alluvial fan environment (Appendix 1). Frequent and occasionally prolonged changes in *G. sacculifer* preservation within the core resulted in large data gaps, as much as ~40kyr, within both the SST and $\delta^{18}O_{SW}$ records (Figure 6). The gaps make some features within the record difficult to identify and cause some ambiguity around poorly defined glacial/interglacial peaks consisting of only a few data points. The gaps significantly affected the interpretation of the $\delta^{18}O_{SW}$ record, making it difficult to draw conclusions from comparisons with other individual records. When compared with the LR04 global stack, there were few discernable glacial features within the $\delta^{18}O_{SW}$ record (Lisiecki & Raymo, 2005). The seasonal changes in local evaporation/precipitation also has an influence on $\delta^{18}O_{SW}$, further masking the glacial signal in comparison to a benthic record. There does not appear to be any long-term trends affecting the $\delta^{18}O_{SW}$ mean during the MPT, but the poorly defined peaks make it difficult to accurately gauge changes in amplitude (Figure 6). Despite the limitations of the $\delta^{18}O_{SW}$ record in recording the characteristics of the Mid-Pleistocene, the SST record did provide insight into the paleoceanographic conditions at site U1452 and the tropics during the MPT.

Mid-Pleistocene Sea Surface Temperature

The importance of SST in the southern Bay of Bengal stems from the influx of warm equatorial surface water due to the Southwest Monsoon Current, which generates the latent heat and atmospheric convection that supports the South Asian Summer Monsoon (Figure 2; Schott et al., 2009; Zhisheng et al., 2001). Modern observations show that tropical surface temperatures between 26 - 30°C is the ideal range for peak atmospheric convection (Tompkins, 2001). Surface temperatures in the southern Bay of Bengal averaged 28.9°C across the Mid-Pleistocene, well within the temperature range for peak convection (Figure 7). However, it should be noted that the record's mean is dependent on the chosen calibration and alternate calibrations would shift the mean (Appendix 2; Figure A2.3). However, characteristics of the record such as amplitude and slope, would remain consistent regardless of the calibration chosen. In all calibrations tested (Figure A2.3), SST conditions at site U1452 do not exhibit a significant change in the mean across the MPT that would suggest a temperature trend (Figure 7). In order to determine if the chosen ΔCO_3^{2-} dissolution calibration was appropriate, we initially compared the mean SST to modern oceanographic observations that mean SST be 29 ± 0.8°C average (Levitus, 1982). In addition to comparing the mean modern SST observations, we evaluated at the core-top data from other sites along 8°N (Fritz-Endres, 2016). Expedition 354 sites U1454 and U1449 core-top analysis observed similar Mg/Ca SST means of 29.8 ± 2.9°C and 27.9 ± 3.6°C, respectively (Fritz-Endres, 2016). While this similarity between modern observations & core-top data indicates foraminiferal Mg/Ca is a good estimation of SST for these sites, we also looked at the Mg/Ca SST data from the last ~200kyr to see if SST changed significantly from modern observations. The Mg/Ca SST record from 3 – 170ka displayed an average of 28.4°C (Holmes & Dekens, 2017), suggesting there is not a significant difference between modern SST and Cenozoic paleotemperatures in the Southern Bay of Bengal. Based on these comparisons, we believe the chosen ΔCO_3^{2-} dissolution calibration is appropriate and SST during the Mid-Pleistocene were likely within range to support of peak atmospheric convection (Tompkins, 2001).

In order to determine the how U1452 SST contributes to our understanding of the tropical response to the MPT, we compared the record to other tropical records the Indian

Ocean and equatorial Pacific (Table 2). While there are few Mid-Pleistocene records in the Indian Ocean, we were able to compare site 1452 to the nearby ODP site 758 (Dekens, 2007). ODP site 758 has a mean SST of 28.3°C, which is reasonable considering the site's proximity to site U1452 (Table 2). The warmest tropical SST's were recorded in the W. equatorial Pacific ODP site 806 (29.5°C; Wara et al., 2005) and Coral Sea site MD06-3018 (30.2°C; Russon et al., 2010). These tropical Mg/Ca SST records are also stable through the Mid-Pleistocene and all means fall between ~28 – 30°C with no observed temperature trends (Table 2). However, records in cooler upwelling zones have notably cooler mean SST, such as E. Pacific ODP site 847's mean SST of 24.1°C (Wara et al., 2005). The alkenone SST record from the Eastern equatorial Pacific ODP site 846 also displays cooler mean SST of 24°C and a notable 1.3°C cooling trend from 0.9 – 1.3Ma (Medina-Elizalde & Lea, 2005). As the MPT is affecting glacial frequency, the cooling SST trend at ODP 847 may be a result upwelling intensification due to of deep-ocean changes. The stable tropical SST's in non-upwelling zones like the Southern Bay of Bengal suggests that while the global climate shifted to a 100kyr glacial frequency, there was not a significant effect on insolation in the tropics.

While site U1452's SST record remains warm and stable, other local records indicate the South Asian Monsoon weakened during the MPT (Sun et al., 2006; Weber & Reilly, 2018). As the world's glacial cycles shifted into 100kyr dominance, the prevalence of larger, persistent ice sheets increased global aridity across the MPT (Raymo et al., 1997). A study of Chinese loess soil grain size suggests the summer monsoon weakened while the winter monsoon, characterized by northeasterly winds that bring dry, cold air to the Bay of Bengal, strengthened over the MPT (Sun et al., 2006; Weber & Reilly, 2018). This observation is supported by the reduction in turbidite deposition in the site U1452 core lithology resulting in the exceptional preservation of the Mid-Pleistocene hemipelagic interval used in this study (Weber & Reilly, 2018). Frequent turbidite deposits can be associated with changes in sea level and periods of increased suspended sediment in river discharge, potentially from precipitation events accelerating erosion (Jena et al., 2016; Shanmugam et al., 1985; Weber & Reilly, 2018). Glacial sea level low-stands act as periods of fan growth due to the exposure of shelf material to erosion and proximity of river-mouths to the active channel head (Shanmugam et al., 1985). The currents occur when the accumulated sediments collapse as a gravity-driven flow that propagates the sediment down-channel to be deposited on channel levees and the surrounding fan as turbidites (Appendix 1; Jena et al., 2016; Shanmugam et al., 1985). In spite of more persistent glacial intervals, the decrease in turbidite activity suggests either the active channel migrated away from the 354 transect or more arid conditions weakened precipitation-driven erosion in the Himalayas. A weaker monsoon could result in a decrease in precipitation and fluvial transport of sediment to active channel head (Weber & Reilly, 2018). It should be noted that while the lithology and loess records pose interesting questions, site U1452 is too far south to directly record any changes related to the monsoon. Future work will compare those records and records from the 354 transect to the results of northern Bay of Bengal expedition 353, which is directly studying the evolution of the monsoon system through the Quaternary. Ideally, the combination will provide a better regional understanding of monsoon evolution through the Pleistocene.

Mid-Pleistocene Benthic Conditions

The benthic $\delta^{18}O$ record was created to reconstruct the glacial record and evaluate the site's stratigraphic age model by comparing it with the LR04 global benthic $\delta^{18}O$ stack (Figure 8; Lisiecki & Raymo, 2005). The site U1452's age model consists of interpolation between 23 stratigraphic tie points, including 5 magnetic reversals, the Oldest Toba Tephra unit, and points derived from sediment lightness (L*) and magnetic susceptibility (MS) records (Figure 3; Table 1; Weber & Reilly, 2018). The age model indicates core 37F spans the Middle Pleistocene (0.84 – 1.27Ma) and contains the Mid-Pleistocene Transition (~0.8-1.3Ma) (Weber & Reilly, 2018; Figure 3; Table 1).

We compared site U1452's benthic $\delta^{18}O$ record to other tropical benthic $\delta^{18}O$ records and the LR04 global benthic $\delta^{18}O$ stack to evaluate the MPT's effect on the Indian Ocean (Figure 8; Table 3). Various benthic $\delta^{18}O$ records from the Pacific (Mix et al., 1995; Shackleton et al., 1990), Atlantic (Bickert et al., 1997; K. Billups & Schrag, 2002; Franz, 1999; Venz & Hodell, 2002), South China Sea (Clemens & Prell, 2003), and Indian Ocean (Chen et al., 1995; Clemens et al., 1996) were compared to the site U1452 *U. peregrina* $\delta^{18}O$ record (Table 3). All records show the Mid-Pleistocene glacial cycles observed in the LR04 global stack, but the site U1452 record has the most significant temporal offset from the LR04 stack and other benthic $\delta^{18}O$ records. The other $\delta^{18}O$ records average approximately 3.9‰, consistent with site U1452 and LR04 (Table 3;

Lisiecki & Raymo, 2005). Since the various $\delta^{18}O$ records are so similar and most of them are included in the LR04 stack, the LR04 stack is a good comparison record for site U1452 during the MPT (Figure 8).

While our benthic $\delta^{18}O$ record does not extend through ~0.65 - 0.75Ma, when the 100kyr frequency became most pronounced, site U1452's benthic $\delta^{18}O$ record does capture the glacial cycles observed in the LR04 global benthic stack during the MPT (~0.8-1.3Ma) (Lisiecki & Raymo, 2005; Figure 7). While the glacial cycles can be observed in the site U1452 record, the timing is offset from the LR04 stack by ~1kyr to as much as ~20kyr (Figure 7). However, the portions of the U1452 record with the largest temporal offset often occur in the late MPT at interglacial peaks, where there are small gaps in the data set (Figure 7). The interglacial data gaps are due to the low abundance of *U. peregrina* during interglacial periods, as the species prosper primarily during glacial intervals (Wells et al., 1994). As a result, the temporal offsets may be smaller than they appear due to the record missing the true interglacial peak. However, the presence of significant offsets of up to a full precessional cycle (~20kyr) suggests potential error in the age model.

Unlike traditional deep-ocean drill sites, alluvial fans are more complex depositional environments where assuming constant sedimentation between stratigraphic tie points ignores the more erratic deposition of fan sediments via turbidity flows (Appendix 1). While there is evidence of a decrease turbidite activity near Site U1452 at the start of the MPT (France-Lanord et al., 2016b; Weber & Reilly, 2018), the terrestrial component of the hemipelagic intervals indicates some sedimentation via these fan processes is occurring. The terrestrial component is primarily pelagic silts inputted into the water column from more distal turbidite activity rather than deposits of the coarser, sandy turbidite deposits observed pre- and post-MPT (France-Lanord et al., 2016b). Due to the irregular frequency of turbidite deposition, assuming constant sedimentation between tie points creates error in the age model resulting in the observed offset between the site U1452, LR04, and other benthic $\delta^{18}O$ records (Figures 3 & 7). Variability in sedimentation can be due to changes in conditions on glacial-interglacial timescales, such as monsoon erosion and sea level. Internal fan processes, including the lateral migration of the active channel relative to site U1452 or the frequency of turbidity currents, can also affect sedimentation rate on shorter timescales (Appendix 1; Weber & Reilly, 2018). As a result, a variety of factors could be influencing sedimentation rate between tie points and can lead to the offset observed.

Recent work evaluating the use of a global $\delta^{18}O$ stack to improve age control on sediment cores suggests error in the age model may not be the only factor contributing to the offset between site U1452 and the LR04 benthic records (Lisiecki & Stern, 2016). Individual benthic records are not synchronous, as previously assumed, and different sites can record the effects of the same signal at different times (Lisiecki & Stern, 2016). In regions exposed to a relatively uniform deep-water mass; for example, two Atlantic sites, the timing difference is slight and the method of aligning to a global stack is appropriate (Lisiecki & Stern, 2016). However, the LR04 stack is primarily composed of Atlantic and Pacific sites where the deep-water masses are distinct from the Indian Ocean. Due to the deep-water circulation, a glacial-interglacial signal recorded in the Atlantic deep-water $\delta^{18}O$ could take thousands of years to be incorporated into the Indian Ocean's deep-water mass and recorded. Therefore, aligning records to a global average, such as site U1452 to the LR04 stack, ignores significant regional age differences between sites in different ocean basins (Lisiecki & Stern, 2016). The diachronous nature of benthic $\delta^{18}O$ is believed to contribute as much as a 4ky difference between individual records' age models, but there is some debate regarding the velocity of deep-ocean circulation (Lisiecki & Stern, 2016). However, many of the offsets observed in the site U1452 record are larger than 4kyr suggesting that a combination of factors is likely the cause. Future work will be able to compare other $\delta^{18}O$ records and age models from the Bay of Bengal expeditions 353 and 354 to $\delta^{18}O$ stacks that account for these regional differences, such LS16 (Lisiecki & Stern, 2016), and better identify the source of the site U1452 offset.

Mid-Pleistocene Benthic $\delta^{13}C$

Similar to the $\delta^{18}O$ record, the site U1452 $\delta^{13}C$ record also shows characteristics of the MPT. Atlantic records (Alonso-Garcia et al., 2011; Raymo et al., 1997) show the MPT shift in glacial frequency observed in $\delta^{18}O$ record had long term effects on global sea level and terrestrial aridity during the Mid-Pleistocene. During the more persistent Mid-Late Pleistocene glacial intervals, the continents became more arid and sea level dropped (Elderfield et al., 2012). Lower sea level allowed for the erosion of continental shelf carbon, primarily isotopically light $\delta^{13}C$ marine carbonate material, into the deep ocean (Elderfield et al., 2012). Atlantic records for the MPT observed this change in the deep ocean carbon reservoir as an approximately 0.3‰ decrease in deep-ocean $\delta^{13}C$ between 0.9 – 1.0Ma (Raymo et al., 1997). Due to the thermohaline circulation of North Atlantic Deep Water and Antarctic Bottom Water into the Indian Ocean, the benthic conditions at site U1452 should reflect these global changes to deep-ocean $\delta^{13}C$, as well as a local signal.

The site U1452 *U. peregrina* $\delta^{13}C$ record also decreases by ~0.3‰ similar to the Atlantic records (Figure 8; Alonso-Garcia et al., 2011; Raymo et al., 1997). While deep-ocean circulation could be the source of the $\delta^{13}C$ signal, it is important to note the Bay of Bengal is not a strong upwelling zone and local processes would also contribute to local deep-ocean chemistry. In other records, the ~0.3‰ decrease is attributed to the more pronounced sea-level low-stands during the transition to 100kyr dominance that exposed continental shelf material and increased the export of isotopically light carbon to the deep-ocean (Raymo et al., 1997). Even though the Bay of Bengal is not a strong upwelling zone, this signal would have been supported by similar changes in Bay of Bengal sea level and the transport of $\delta^{13}C$ depleted shelf sediment from continental shelves to the deep-ocean via the fan's turbidity currents. Whether the source of this $\delta^{13}C$ signal is the result of global deep-water circulation or local processes, it is clear that benthic $\delta^{13}C$ is being affected by processes associated with the MPT. Future work will compare site U1452 sea surface and deep ocean characteristics to other Mid-Pleistocene records from Expeditions 353 and 354 to better understand the evolution of climate, oceanographic, and sedimentary conditions in the Bay of Bengal (Clemens et al., 2015; France-Lanord et al., 2016a).

CONCLUSIONS

In spite of uncertainties relating to the unique alluvial fan environment, this study was able to reconstruct oceanographic conditions at site U1452 during the Mid-Pleistocene. However, there are limitations related to gaps in data due to fluctuations in foraminifera preservation. This primarily affects the *G. sacculifer* $\delta^{18}O_{SW}$ record, as we are unable to observe the glacial-interglacial features in the record. However, the *G. sacculifer* Mg/Ca successfully recorded SST over the Mid-Pleistocene with clear features in spite of data gaps (Figures 5, 7). No long-term temperature trend is observed, consistent with other Mid-Pleistocene SST records from tropical, non-upwelling sites (Table 2). Future work will examine the implications of stable SST's in the Southern Bay of Bengal in relation to the results of Expedition 353's work on monsoon evolution in the Northern Bay of Bengal. Additionally, we hope these record can contribute to the regional understanding of tropical climate evolution as more paleoceanographic records are generated for the Indian Ocean.

The reconstruction of benthic conditions at site U1452 suggests the MPT had greater influence on deep-water chemistry and reveals error in the age model. While the MPT does not appear to be significantly changing surface conditions, the *U. peregrina* record shows a ~0.3‰ decrease in $\delta^{13}C$ characteristic of Mid-Pleistocene changes in deep-ocean carbon (Figure 8). The global ~0.3‰ decrease of deep-ocean $\delta^{13}C$ is attributed more persistent glacial intervals during 100kyr cycles and the resultant sea-level low stands exposing continental shelves to erosion (Raymo et al., 1997). When compared to the LR04 global $\delta^{18}O$ stack, the *U. peregrina* $\delta^{18}O$ record clearly records the Mid-Pleistocene glacial cycles. However, the significant (up to ~20kyr) offsets from the LR04 stack suggests error in the site U1452 age model (Lisiecki & Raymo, 2005). This error is likely a combination of fluctuations in sedimentation between tie points and error in comparing $\delta^{18}O$ records in different ocean basins (Lisiecki & Stern, 2016; Weber & Reilly, 2018). We will continue to work with the Expedition 354 paleomagnetism team to reduce this error, ultimately refining the age models for this interval in all Expedition 354 sites (Weber & Reilly, 2018). Future work will incorporate the *U. peregrina* $\delta^{18}O$ record into the age model by generating additional tie points with the LR04 stack or the basin-adjusted LS16 $\delta^{18}O$ stack if it is extended into the Pleistocene (Lisiecki & Raymo, 2005; Lisiecki & Stern, 2016).

REFERENCES

Alonso-Garcia, M., Sierro, F. J., Kucera, M., Flores, J. A., Cacho, I., & Andersen, N. (2011). Ocean circulation, ice sheet growth and interhemispheric coupling of millennial climate variability during the mid-Pleistocene (ca 800-400ka). *Quaternary Science Reviews*, *30*(23–24), 3234–3247. https://doi.org/10.1016/j.quascirev.2011.08.005

Anand, P., Elderfield, H., & Conte, M. H. (2003). Calibration of Mg/Ca thermometry in planktonic foraminifera from a sediment trap time series. *Paleoceanography*, *18*(2), n/a-n/a. https://doi.org/10.1029/2002PA000846

Barker, S., Greaves, M., & Elderfield, H. (2003). A study of cleaning procedures used for foraminiferal Mg/Ca paleothermometry. *Geochemistry, Geophysics, Geosystems*, *4*(9), 1–20. https://doi.org/10.1029/2003GC000559

Bé, A. W. H., Spero, H. J., & Anderson, O. R. (1982). Effects of symbiont elimination and reinfection on the life processes of the planktonic foraminifer Globigerinoides sacculifer. *Marine Biology*, *70*(1), 73–86. https://doi.org/10.1007/BF00397298

Bemis, B. E., Spero, H. J., Bijma, J., & Lea, D. W. (1998). Reevaluation of the oxygen isotopic composition of planktonic foraminifera: Experimental results and revised paleotemperature equations. *Paleoceanography*, *13*(2), 150–160. https://doi.org/10.1029/98PA00070

Bickert, T., Curry, W., & Wefer, G. (1997). Late Pliocene to Holocene (2.6-0 Ma) western equatorial Atlantic deep-water circulation: Inferences from benthic stable isotopes. *Proceedings of the Ocean Drilling Program, Scientific Results*, *154*, 239–254. Retrieved from http://cat.inist.fr/?aModele=afficheN&cpsidt=2134271

Billups, K., Ravelo, A. C., & Zachos, J. C. (1998). Early Pliocene deep water circulation in the western equatorial Atlantic: Implications for high-latitude climate change. *Paleoceanography*, *13*(1), 84–95. https://doi.org/10.1029/97PA02995

Billups, K., & Schrag, D. P. (2002). Paleotemperatures and ice volume of the past 27 Myr revisited with paired Mg/Ca and 18O/16O measurements on benthic foraminifera. *Paleoceanography*, *17*(1), 1003. https://doi.org/10.1029/2000PA000567

Boyle, E. A., & Keigwin, L. D. (1985). Comparison of Atlantic and Pacific paleochemical records for the last 215,000 years: changes in deep ocean circulation and chemical inventories. *Earth and Planetary Science Letters*, *76*(1–2), 135–150. https://doi.org/10.1016/0012-821X(85)90154-2

Brummer, G. J. A., Hemleben, C., & Spindler, M. (1986). Planktonic foraminiferal ontogeny and new perspectives for micropalaeontology. *Nature*, *319*(6048), 50–52. https://doi.org/10.1038/319050a0

Channell, J. E. T., Hodell, D. A., & Curtis, J. H. (2016). Relative paleointensity (RPI) and oxygen isotope stratigraphy at IODP Site U1308: North Atlantic RPI stack for 1.2-2.2 Ma (NARPI-2200) and age of the Olduvai Subchron. *Quaternary Science Reviews*, *131*, 1–19. https://doi.org/10.1016/j.quascirev.2015.10.011

Channell, J. E. T., Hodell, D. A., Singer, B. S., & Xuan, C. (2010). Reconciling astrochronological and $^{40}Ar/^{39}Ar$ ages for the Matuyama-Brunhes boundary and late Matuyama Chron. *Geochemistry, Geophysics, Geosystems*, *11*(12), 1–21. https://doi.org/10.1029/2010GC003203

Chen, J., Farrell, J., Murray, D., & Prell, W. (1995). Timescale and paleoceanographic implications of a 3.6 m.y. oxygen isotope record from the northeast Indian Ocean (Ocean Drilling Program site 758). *Paleoceanography*, *10*, 21–47.

Clemens, S. C., Kuhnt, W., & Levay, L. J. (2015). Expedition 353 Preliminary Report, (November 2014).

Clemens, S. C., Murray, D. W., & Prell, W. L. (1996). Nonstationary Phase of the Plio-Pleistocene Asian Monsoon. *Science*, *274*(5289), 943–948.

Clemens, S. C., & Prell, W. L. (2003). 3 . D Ata R Eport : O Xygen and C Arbon I Sotopes From S Ite 1146 , N Orthern S Outh C Hina S Ea 1. *Earth*, *184*(April).

Clift, P. D., Hodges, K. V., Heslop, D., Hannigan, R., Van Long, H., & Calves, G. (2008). Correlation of Himalayan exhumation rates and Asian monsoon intensity. *Nature Geoscience*, *1*(12), 875–880. https://doi.org/10.1038/ngeo351

Dekens, P. S. (2007). *Characterizing upwelling regions in the Indo-Pacific Warm Pool in the Early Pliocene Warm Period.* University of California, Santa Cruz. Unpublished Raw Data.

Dekens, P. S., Lea, D. W., Pak, D. K., & Spero, H. J. (2002). Core top calibration of Mg/Ca in tropical foraminifera: Refining paleotemperature estimation. *Geochemistry, Geophysics, Geosystems*, *3*(4), 1–29. https://doi.org/10.1029/2001GC000200

Elderfield, H., Ferretti, P., Greaves, M., Crowhurst, S. J., McCave, I. N., Hodell, D. a, & Piotrowski, A. M. (2012). Evolution of Ocean Temperature. *Science (New York, N.Y.)*, *337*(August), 704–709. https://doi.org/10.1594/PANGAEA.786205

Elderfield, H., Yu, J., Anand, P., Kiefer, T., & Nyland, B. (2006). Calibrations for benthic foraminiferal Mg / Ca paleothermometry and the carbonate ion hypothesis, *250*, 633–649. https://doi.org/10.1016/j.epsl.2006.07.041

France-lanord, C., Spiess, V., & Klaus, A. (2015). Expedition 354 Preliminary Report Bengal Fan Neogene and late Paleogene record of Himalayan orogeny and climate : a transect across the Middle Bengal Fan, (March). https://doi.org/10.14379/iodp.pr.354.2015

France-Lanord, C., Spiess, V., Klaus, A., Adhikari, R. R., Adhikari, S. K., Bahk, J.-J., … Yoshida, K. (2016a). Expedition 354 Methods. *Proceedings of the International Ocean Discovery Program*, *354*(September), 1–35. https://doi.org/10.14379/iodp.proc.354.102.2016

France-Lanord, C., Spiess, V., Klaus, A., Adhikari, R. R., Adhikari, S. K., Bahk, J.-J., … Yoshida, K. (2016b). Expedition 354 summary, *354*(September), 1–35. https://doi.org/10.14379/iodp/proc.354.101.2016

France-Lanord, C., Spiess, V., Klaus, A., Adhikari, R. R., Adhikari, S. K., Bahk, J.-J., … Yoshida2, K. (2016). *Site U1452 Proceedings of the International Ocean Discovery Program Volume 354.*

Franz, S. (1999). *Pliozäne Zeitreihen zur Rekonstruktion der Tiefenwasserzirkulation und der siliziklastischen Amazonasfracht im äquatorialen Westatlantik.*

Fritz-Endres, T. (2016). *Sedimentary controls on foraminifera deposition in the Bay of Bengal.* San Francisco State University.

Goswami, B. N. (2005). South Asian monsoon. In *Intraseasonal Variability in the Atmosphere-Ocean Climate System (Second Edition)* (Vol. 1, pp. 21–72). https://doi.org/10.1007/978-3-642-13914-7_2

Herbert, T. D., Peterson, L. C., Lawrence, K. T., & Liu, Z. (2010). Tropical Ocean Temperatures Over the, *328*(June), 1530–1535. https://doi.org/10.1126/science.1185435

Holmes, B., & Dekens, P. S. (2017). *Ocean Conditions in the Southern Bay of Bengal during the Last Glacial Cycle*. Senior Thesis. San Francisco State University. Unpublished Raw Data.

Huybers, P. (2006). Early Pleistocene glacial cycles and the integrated summer insolation forcing. *Science (New York, N.Y.)*, *313*(5786), 508–511. https://doi.org/10.1126/science.1125249

Huybers, P. (2007). Glacial variability over the last two million years: an extended depth-derived agemodel, continuous obliquity pacing, and the Pleistocene progression. *Quaternary Science Reviews*, *26*(1–2), 37–55. https://doi.org/10.1016/j.quascirev.2006.07.013

Jena, B., Kurian, P. J., & Avinash, K. (2016). Morphology of submarine channel-levee systems in the eastern Bay of Bengal near Andaman region. *Journal of Coastal Conservation*, 211–220. https://doi.org/10.1007/s11852-016-0431-2

Kessarkar, P. M., Rao, V. P., Ahmad, S. M., Patil, S. K., Kumar, A. A., Babu, G. A., … Rajan, R. S. (2005). Changing sedimentary environment during the Late Quaternary : Sedimentological and isotopic evidence from the distal Bengal Fan, *52*, 1591–1615. https://doi.org/10.1016/j.dsr.2005.01.009

Levitus, S. (1982). Climatological atlas of the world ocean. *US Government Printing Office, Washington DC, NOAA Profe*(13).

Lisiecki, L. E., & Raymo, M. E. (2005). A Pliocene-Pleistocene stack of 57 globally distributed benthic ?? 18O records. *Paleoceanography*, *20*(1), 1–17. https://doi.org/10.1029/2004PA001071

Lisiecki, L. E., & Raymo, M. E. (2007). Plio–Pleistocene climate evolution: trends and transitions in glacial cycle dynamics. *Quaternary Science Reviews*, *26*, 56–69. https://doi.org/10.1016/j.quascirev.2006.09.005

Lisiecki, L. E., & Stern, J. V. (2016). Regional and global benthic δ18O stacks for the last glacial cycle. *Paleoceanography*, *31*(10), 1368–1394. https://doi.org/10.1002/2016PA003002.Received

Martin, P. A., & Lea, D. W. (2002). A simple evaluation of cleaning procedures on fossil benthic foraminiferal Mg/Ca. *Geochemistry, Geophysics, Geosystems*, *3*(10), 1–8. https://doi.org/10.1029/2001GC000280

Medina-Elizalde, M., & Lea, D. W. (2005). The mid-Pleistocene transition in the tropical Pacific. *Science (New York, N.Y.)*, *310*(5750), 1009–1012. https://doi.org/10.1126/science.1115933

Mix, A. C., Pisias, N. G., Rugh, W., Wilson, J., Morey, A., & Hagelberg, T. K. (1995). Benthic Foraminifer Stable Isotope Record from Site 849 (0-5 Ma): Local and Global Climate Changes. *Proceedings of the Ocean Drilling Program, 138 Scientific Results*, *138*. https://doi.org/10.2973/odp.proc.sr.138.120.1995

Pena, L. D., Calvo, E., Cacho, I., Eggins, S., & Pelejero, C. (2005). Identification and removal of Mn-Mg-rich contaminant phases on foraminiferal tests: Implications for Mg/Ca past temperature reconstructions. *Geochemistry, Geophysics, Geosystems*, *6*(9). https://doi.org/10.1029/2005GC000930

Raymo, M. E., Oppo, D. W., & Curry, W. (1997). The mid-Pleistocene climate transition: A deep sea carbon isotopic perspective records from the deep ocean, extending back examined in order to constrain decrease in mean. *Paleoceanography*, *12*(4), 546–559.

Raymo, M., Lisiecki, L., & Nisancioglu, K. H. (2006). RESEARCH ARTICLES Plio-Pleistocene Ice Volume, Antarctic Climate, and the Global, *c*(July), 492–496.

Rosenthal, Y., Lohmann, G. P., Lohmann, K. D., & Sherrell, R. M. (2000). Incorporation and preservation of Mg in Gs. sacculifer: implications for reconstructing the temperature and oxygen isotopic composition of seawater. *Paleoceanography*, *145*(1), 135–145.

Russon, T., Elliot, M., Sadekov, A., Cabioch, G., Corrge, T., & De Deckker, P. (2010). Inter-hemispheric asymmetry in the early Pleistocene Pacific warm pool. *Geophysical Research Letters*, *37*(11), 1–5. https://doi.org/10.1029/2010GL043191

Schott, F. A., Xie, S.-P., & McCreary Jr, J. P. (2009). Indian Ocean Circulation and Climate Variability. *Reviews of Geophysics*, *47*(2007), 1–46. https://doi.org/10.1029/2007RG000245.1.INTRODUCTION

Shackleton, N. J. (1974). Attainment of isotopic equilibrium between ocean water and the benthonic foraminifera geuns Uvigerina: Isotopic changes in the ocean during the last glacial. *Colloques Internationaux Du C.N.R.S.*, *219*, 203–210.

Shackleton, N. J., Berger, A., & Peltier, W. R. (1990). An alternative astronimical calirbation of the lower Pleistocene timescale based on ODP Site 677. *Transactions of the Royal Society of Edinburgh, Earth Scie*(81), 251–261.

Shanmugam, G., Moiola, R. J., & Damuth, J. E. (1985). Chapter 5 - Eustatic Control of Submarine Fan Development. In *Submarine Fans and Related Turbidite Systems* (pp. 23–28).

Sun, Y., Lu, H., & An, Z. (2006). Grain size of loess, palaeosol and Red Clay deposits on the Chinese Loess Plateau: Significance for understanding pedogenic alteration and palaeomonsoon evolution. *Palaeogeography, Palaeoclimatology, Palaeoecology*, *241*(1), 129–138. https://doi.org/10.1016/j.palaeo.2006.06.018

Tompkins, A. (2001). On the relationship between tropical convection and sea surface temperature. *Journal of Climate*, *14*, 633–637. https://doi.org/10.1175/1520-0442(2001)014<0633:OTRBTC>2.0.CO;2

Venz, K., & Hodell, D. (2002). *New evidence for changes in Plio-Pleistocene deep water circulation from Southern Ocean ODP Leg 177 Site 1090. Palaeogeog. Palaeoclim. Palaeoecol.* (Vol. 2002). https://doi.org/10.1016/S0031-0182(01)00496-5

Wara, M. W., Ravelo, A. C., & Delaney, M. L. (2005). Climate change: Permanent El Niño-like conditions during the Pliocene warm period. *Science*, *309*(5735), 758–761. https://doi.org/10.1126/science.1112596

Weber, M. E., & Reilly, B. T. (2018). Hemipelagic and turbiditic deposits constrain lower Bengal Fan depositional history through Pleistocene climate, monsoon, and sea level transitions. *Quaternary Science Reviews*, *199*, 159–173. https://doi.org/10.1016/j.quascirev.2018.09.027

Wells, P., Wells, G., Cali, J., & Chivas, A. (1994). Response of deep-sea benthic foraminifera to Late Quaternary climate changes, southeast Indian Ocean, offshore Western Australia. *Marine Micropaleontology*, *23*, 185–229.

Zhisheng, A., Guoxiong, W., Jianping, L., Youbin, S., Yimin, L., Weijian, Z., … Juan, F. (2015). Global Monsoon Dynamics and Climate Change. *Annual Review of Earth and Planetary Sciences*, *43*(1), 29–77. https://doi.org/10.1146/annurev-earth-060313-054623

Zhisheng, A., Kutzbach, J. E., Prell, W. L., & Porter, S. C. (2001). Evolution of Asian monsoons and phased uplift of the Himalaya-Tibetan plateau since Late Miocene times. *Nature*, *411*(6833), 62–66. https://doi.org/10.1038/35075035

APPENDICES

Appendix 1 - Bengal Fan Lithology

The Bay of Bengal contains the largest submarine alluvial fan in the world, extending from the Bengal Delta south to the equatorial Indian Ocean (Figure 1; Jena et al., 2016). The Ganges-Brahmaputra river system deposits 2.2x10^9 tonnes of sediment annually into the upper fan (Jena et al., 2016). Sediment dispersed throughout via gravity driven turbidity currents that occur when bottom water with a dense suspended load and sediment accumulate at the active channel head (Jena et al., 2016). The turbidity currents convey the sediment and suspended load throughout the fan via the active channel and are they primary fan-building mechanism (Jena et al., 2016; Weber & Reilly, 2018). The sediment deposited by turbidity currents are referred to as turbidite sequences, and often consist of an upward fining sequence of sands and clays. Due to the velocity of the flows, turbidites are often associated with stratigraphic unconformities.

Due to the frequency of turbidites and the associated unconformities, a continuous, well-preserved hemipelagic layer at site U1452 is unique within the alluvial fan complex (Figure A1.1). The deposition of a laterally extensive hemipelagic layer across all 354 sites indicates turbidite deposition ceased within the transect from ~0.8 – 1.3Ma (Figure A1.1; France-Lanord et al., 2016b; Weber & Reilly, 2018). The hemipelagic material is a combination of terrigenous and marine sediment from the overlying water column (France-Lanord et al., 2016; Kessarkar et al., 2005). While the deposition of sandy turbidite sequences ceased, distal turbidity flows suspend clouds of pelagic silts and clays in the water column (France-Lanord et al., 2016; Kessarkar et al., 2005). The simultaneous deposition of sediment types in the fan link the terrestrial and marine components in time, allowing studies to link oceanographic and terrestrial records through lithology.

While the alluvial fan environment establishes the terrestrial-marine link and the comparison of different sites in the transect, the fan processes can make it difficult to create an accurate age model. While turbidites and unconformities are not observed in this layer, the sedimentation rate in the fan can be affected by processes related to local and global climate processes (Weber & Reilly, 2018). Glacial cycles can fluctuate local sea level affecting frequency of turbidity currents. Turbidity currents and fan building intensifies when sea level lowers during glacial intervals, which moves the Ganges-Brahmaputra mouth closer to the active channel head (Shanmugam et al., 1985). The evolution of monsoon intensity also influences the rate of erosion inputting sediment to the Ganges-Brahmaputra watershed. Internal fan processes, such as the location of the active channel, determines sedimentation (Jena et al., 2016; Shanmugam et al., 1985). The fan's active channel migrates laterally across the fan over time, fluctuating the sedimentation rate based on site proximity to the active channel (Jena et al., 2016; Shanmugam et al., 1985). These mechanisms affecting sedimentation rate are important, as stratigraphic age models interpolate between known tie points and assume constant sedimentation. The amount of tie points reduces error and the age model for site U1452 is a combination of tie points from paleomagnetic data and sediment lightness (L*) (Weber & Reilly, 2018).

The hemipelagic unit is characterized by the presence of the Jamarillo magnetic reversal subchron, placing the unit in the Mid-Pleistocene (France-Lanord et al., 2016). In the thicker hemipelagic units, such as Site 1452, age control is improved due to the presence of five magnetic reversals boundaries identified as the Bruhnes, Matuyama, Jaramillo, and Cobb Mountain subchrons (Table 1; France-Lanord et al., 2016; Weber & Reilly, 2018). These reversals, in addition to the oldest Toba Tephra unit and tie points derived from the L* record, age the site U1452 layer in the Mid-Pleistocene between ~0.84 – 1.27Ma (Table 1; Weber & Reilly, 2018). Accurate age models at each site are crucial, as the changing thickness and core depth at each site indicates varying sedimentation rates and the evolution fan topography. Therefore, other sites' age models were calibrated to site U1452, which had the best age control for the interval (Weber & Reilly, 2018).

Appendix 2 – SST Calibration

The Mg/Ca *G. sacculifer* shell calcite is a commonly used proxy for SST, as the Mg/Ca is determined by the water temperature during shell calcification. However, Mg/Ca trace metal analysis is highly susceptible to bias from contamination and individual shell chemistry and these must be assessed prior to calibration to SST (Barker et al., 2003). While magnesium is a common trace metal found in lab supplies, the samples were cleaned in a dust-free, While the shells are gently cracked open and thoroughly cleaned using oxidative and reductive techniques (Boyle & Keigwin, 1985), small amounts of residual clays, organics, or metals can greatly bias the resulting Mg/Ca values. While analyzing the samples for Mg/Ca, we also measured Mn/Ca as a test for contaminated samples. Increased levels of both Mn/Ca and Mg/Ca is a strong indicator of contamination. The low R^2 value, 0.008, for a scatter plot of Mg/Ca vs. Mg/Ca did not suggest contamination (Figure A2.1).

Another source of bias stems from insufficient homogenization of the bulk samples, allowing individual shell chemistry to influence the Mg/Ca results. A positive correlation between average foraminifera shell mass and Mg/Ca could indicate bulk samples with a higher average shell mass are biased towards high Mg/Ca, not that there is a true increase in temperature. The total weight (mg) for each bulk sample was divided by the number of G. sacculifer shells used to generate the average foraminifera shell mass for that sample. This data set was plotted against the Mg/Ca values to evaluate if there is any trend or correlation between the two variables (Figure A2.2). The low R^2 value of 0.06 indicates there is not a significant correlation between shell mass and Mg/Ca for the site 1452 record (Figure A2.2).

The substitution of Mg^{2+} for Ca^{2+} during the precipitation of foraminifera shell calcite has a positive, exponential relationship to water temperature (Anand et al., 2003). This relationship can be used to derive an SST record from the Mg/Ca data,

$$Mg/Ca = B^{(AT)}$$

where the constants A and B are determined by variations between foraminifera species and T represents calcification temperature (Anand et al., 2003). However, at increased water depths the shell calcite's Mg/Ca can be affected by the preferential dissolution of magnesium rich shell calcite. If the effects of dissolution are not accounted for in the calibration of Mg/Ca to SST, the values will be biased to underestimate the true temperature. IODP Expedition 354 site 1452 was located at a water depth of ~3670m, a depth where the effects of shell calcite dissolution must be considered.

In addition to the general calibration (Anand et al., 2003), two calibrations were applied to correct for dissolution based on water depth and carbonate ion saturation (ΔCO_3^{2-}) (Figure A2.3; Dekens et al., 2002). When comparing the three calibration methods, the general calibration had an SST average of 24.7°C was significantly lower than the modern average of 29 ± 0.8°C (Figure A2.3; Levitus, 1982). A lower mean was expected, as the general calibration does not account for the preferential dissolution of magnesium rich portions of the shell. As dissolution is a function of carbonate ion saturation in the water column, the other calibrations corrected for dissolution using ΔCO_3^{2-} (1) and water depth (2), which is a good proxy for ΔCO_3^{2-} below 1500m (Dekens et al., 2002).

(1) $SST = [\ln((Mg/Ca)/(0.31))/(0.084)] - (0.048*\Delta CO_3^{2-}) \qquad (\Delta CO_3^{2-} = 0.24)$

(2) $SST = [(\ln((Mg/Ca)/(0.37))/(0.09)] + [0.36*(\text{water depth km})] + 2$

As expected, the two calibrations correcting for dissolution increased the mean SST, with the ΔCO_3^{2-} record averaging 28.9°C and the water depth record averaging 28.3°C (Figure A2.3). When deciding between the two calibrations, it must be considered that water depth is a proxy for ΔCO_3^{2-}. Additionally, there is are different water depth boundaries in the equatorial Atlantic (~2.8km) and the equatorial Pacific (~1.6km) that determine when sediment lies at a depth where a dissolution correction should be applied. In order to maintain the relationship between Mg/Ca and SST, the calibration equations are the same, but there is a temperature correction for the Pacific that accounts for this difference. We chose the equatorial Pacific depth calibration equation, as there is not a correction for the equatorial Indian Ocean and water is exchanged between the two basins through the Maritime Continent. While the two dissolution records are similar, the ΔCO_3^{2-} calibration was chosen to generate site 1452's SST record in order to negate any bias related to water depth's correction by ocean basin (Figure 5).

TABLES

Mid-Pleistocene Age Model

Site	Core	Depth CSF- A (m)	Age (ka)	Sedimentation Rate (cm/ka)	Stratigraphic Tie Point
U1452B	36F	183.20	676.00		
U1452B	36F	183.37	712.00	0.47	
U1452B	37F	184.10	774.00	1.18	Bruhnes/Matuyama
U1452B	37F	184.44	785.60	2.93	Oldest Toba Tephra (OTT)
U1452B	37F	184.85	866.00	0.51	
U1452B	37F	185.23	936.00	0.54	
U1452B	37F	185.56	959.00	1.43	
U1452B	37F	185.71	970.00	1.36	
U1452B	37F	185.88	982.00	1.42	
U1452B	37F	185.96	990.00	1.00	Upper Jaramillo
U1452B	37F	186.34	1014.00	1.58	
U1452B	37F	186.58	1031.00	1.41	
U1452B	37F	187.04	1062.00	1.48	
U1452B	37F	187.10	1071.00	0.67	Lower Jaramillo
U1452B	37F	187.13	1081.00	0.30	
U1452B	37F	187.44	1104.00	1.35	
U1452B	37F	187.55	1114.00	1.10	
U1452B	37F	187.95	1141.00	1.48	
U1452B	37F	188.34	1187.00	0.85	Upper Cobb Mountain
U1452B	37F	188.37	1190.00	1.00	
U1452B	37F	188.56	1208.00	1.06	Lower Cobb Mountain
U1452B	37F	188.71	1215.00	2.14	
U1452B	37F	189.08	1244.00	1.28	
		Average Sedimentation Rate		1.21	

Table 1 A table detailing the Mid-Pleistocene stratigraphic tie points utilized in the site 1452 age model (Weber & Reilly, 2018). The magnetic reversal boundaries and Oldest Toba Tephra deposit are labeled, while the other points are generated using a combination of sediment lightness (L*) and magnetic susceptibility (MS) aligned with the LR04 benthic $\delta^{18}O$ stack (Lisiecki & Raymo, 2005; Weber & Reilly, 2018). The sedimentation rates between tie points and average sedimentation rate are also included.

Mid-Pleistocene Tropical SST

Site	Location	Range (°C)	Mean (°C)
IODP 1452	S. Bay of Bengal	26.9 – 31.2	28.9
ODP 758	N. Indian Ocean	26.4 – 30.3	28.3
ODP 806	W. Equatorial Pacific	27.8 – 31.6	29.5
ODP 847	E. Equatorial Pacific	20.9 – 26.9	24.1
MD06-3018	Coral Sea	28.7 – 32.1	30.2

Table 2 A table comparing site U1452 to Mg/Ca SST records from the tropics, including sites from the Indian and Pacific Oceans. Statistics for all records are limited to the Mid-Pleistocene interval (~0.8 – 1.3Ma) spanned by the U1452 record. The range and mean for each record is listed by site and location including ODP site 758 (Dekens, 2007), ODP site 806 (Wara et al., 2005), ODP site 847 (Wara et al., 2005), and site MD06-3018 (Russon et al., 2010).

Mid-Pleistocene Benthic $\delta^{18}O$

Site	Location	Range (‰)	Mean (‰)
IODP 1452	S. Bay of Bengal	3.2– 4.7	4.0
ODP 758	Indian Ocean	3.4 – 5.0	4.2
ODP 722	Arabian Sea	2.5 – 4.7	4.0
ODP 677	Pacific Ocean	3.0 – 5.1	4.1
ODP 849	Pacific Ocean	3.1 – 4.7	4.0
ODP 1146	South China Sea	3.0 – 4.5	3.9
ODP 1090	Atlantic Ocean	3.4 – 4.8	4.1
ODP 925	Atlantic Ocean	2.8 – 4.9	4.0
LR04	57 Record Stack	3.2 – 4.7	4.0

Table 3 A table comparing the site U1452 *U. peregrina* $\delta^{18}O$ record to other individual benthic $\delta^{18}O$ records and the LR04 stack (Lisiecki & Raymo, 2005). Statistics for all records are limited to the Mid-Pleistocene interval (~0.8 – 1.3Ma) spanned by the U1452 record. The range and mean for each record is listed by site and location including ODP site 758 (Chen et al., 1995), ODP site 722 (Clemens et al., 1996), ODP site 677 (Shackleton et al., 1990), ODP site 849 (Mix et al., 1995), ODP site 1146 (Clemens & Prell, 2003), ODP site 1090 (Venz & Hodell, 2002), and ODP site 925 (Bickert et al., 1997; Billups et al., 1998; Franz, 1999).

FIGURES

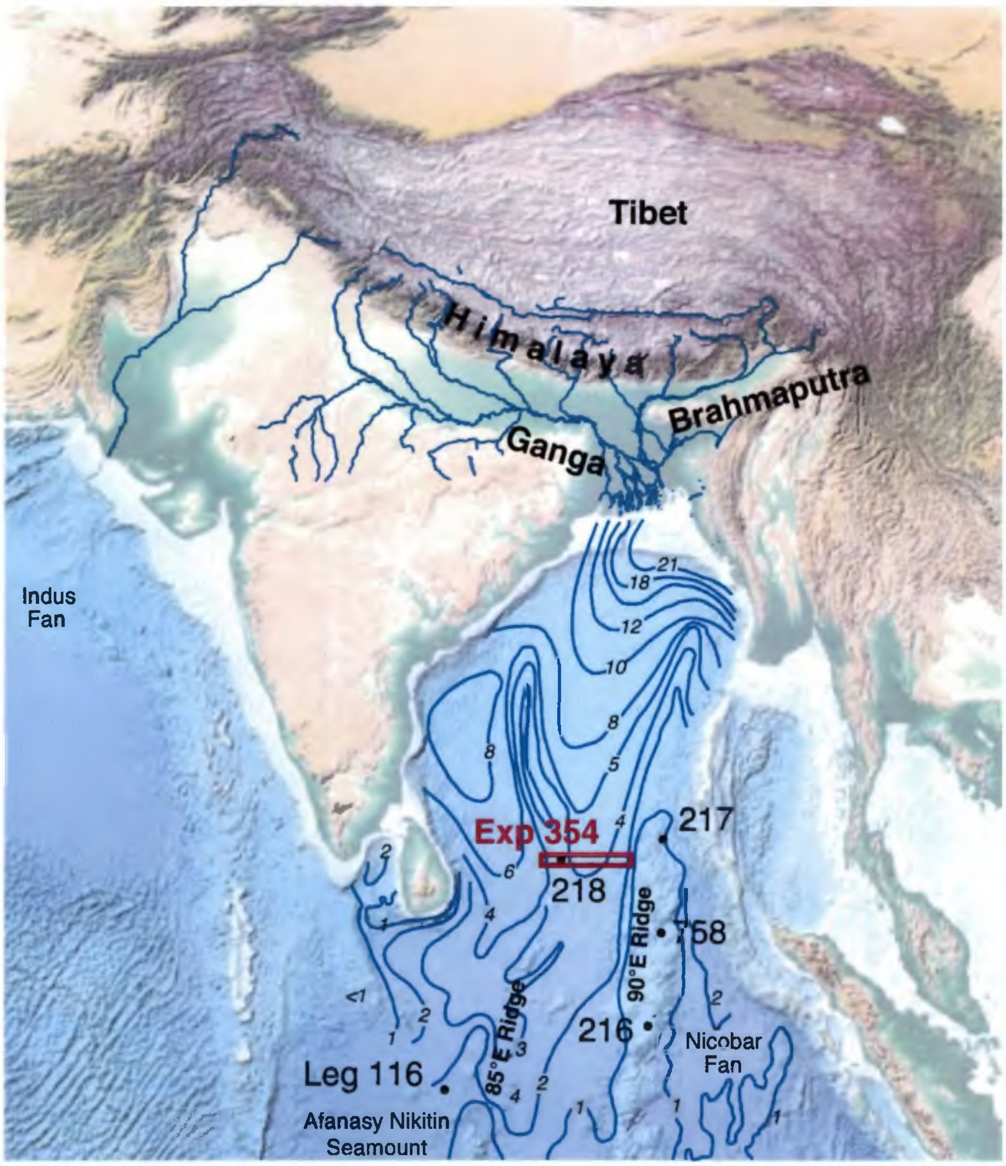

Figure 1 Map showing the east-west transect (red box) along 8°N where International Ocean Discovery Program (IODP) Expedition 354 drilled 7 sites in the Bay of Bengal (France-Lanord et al., 2016a). The cores recovered at these sites are located within the lower Bengal fan complex, blue contour lines represent fan thickness (km), that extends N-S from the Bengal Delta to the equatorial Indian Ocean. The fan is composed of hemipelagic sediment from the water column and surrounding deltas, primarily the Ganges-Brahmaputra watershed in the Himalayan Plateau (Jena et al., 2016).

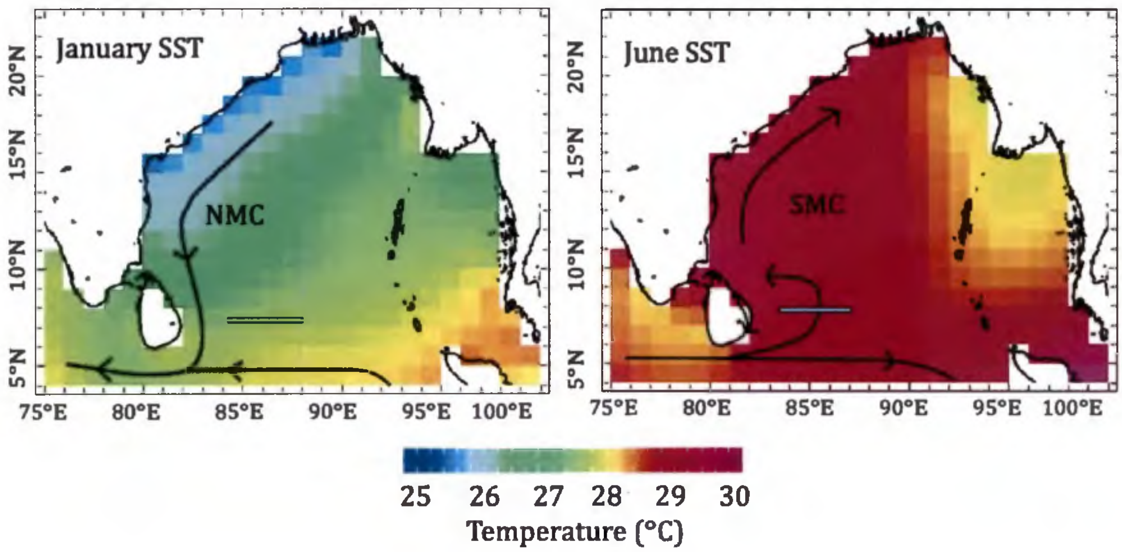

Figure 2 A modern SST map of the Bay of Bengal showing the seasonal currents for January and June, the Northern Monsoon Current (NMC) and Southern Monsoon Current (SMC) (Levitus, 1982; Schott et al., 2009). Expedition 354 is located in the path of the SMC, which transports warm equatorial water to the northern bay in early summer (Schott et al., 2009). The change in SST supplies latent heat to the atmosphere that supports monsoon precipitation over the Himalayan Plateau. The location of the 354 transect is ideally located for studies seeking to understand the link between these oceanographic, climate, and terrestrial conditions.

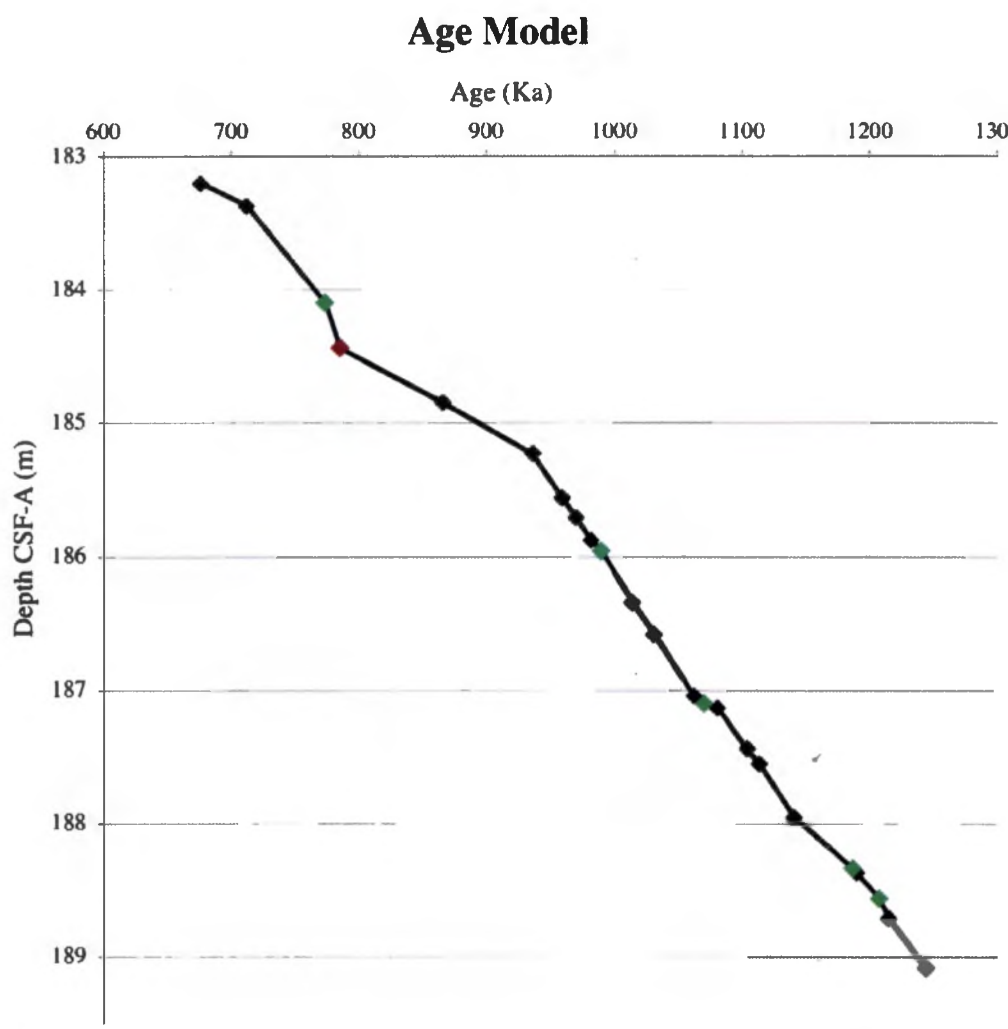

Figure 3 The site U1452 age model, which converts depth to age by interpolating between stratigraphic tie points. The model is composed of the Oldest Toba Tephra (red) and 5 magnetic tie points (blue) including the Brunhes-Matuyama, Upper/Lower Jamarillo and Upper/Lower Cobb Mountain reversals (Channell et al., 2016; Channell et al., 2010; Weber & Reilly, 2018). The sediment lightness (L*) and magnetic susceptibility records were graphically correlated to the LR04 stack (Lisiecki & Raymo, 2005) to create the remaining 17 stratigraphic tie points (grey) (Weber & Reilly, 2018).

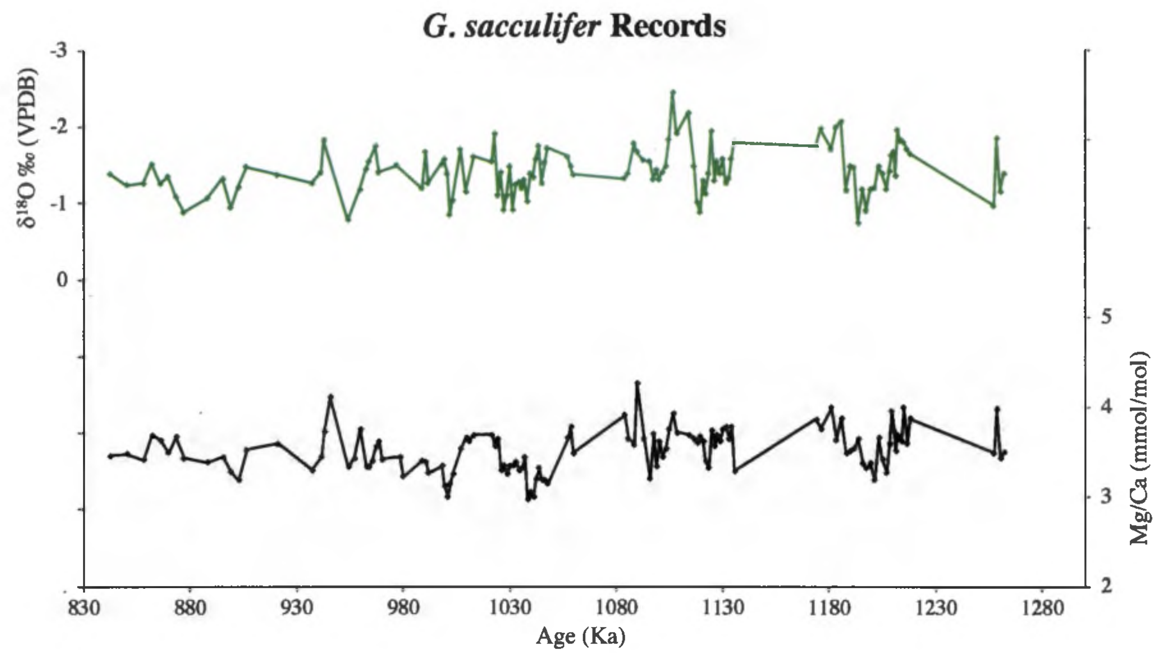

Figure 4 The site U1452 records for *G. sacculifer* shell calcite Mg/Ca (black) and $\delta^{18}O_{CaCO3}$ (green). On the x-axis, core depth has been converted to age (Ka) using the site U1452 age model (Figure 3).

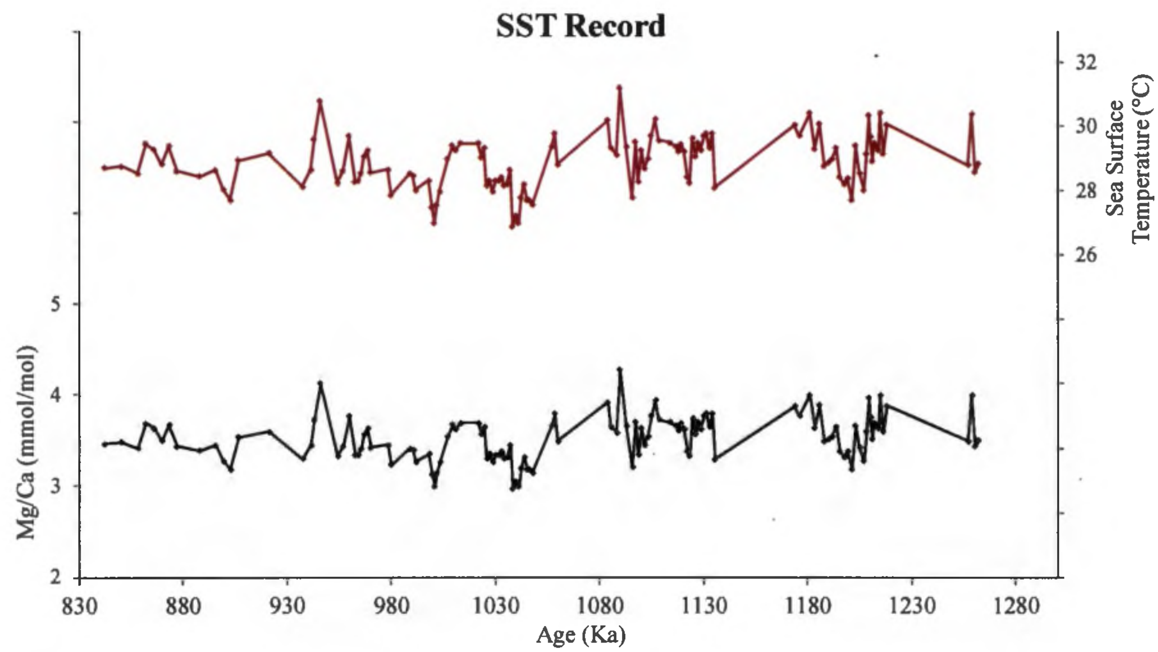

Figure 5 A figure depicting the initial *G. sacculifer* Mg/Ca data (black) and the calibrated Mg/Ca SST (red). The Mg/Ca was calibrated to SST using a calibration equation that corrects for the dissolution of shell calcite by using carbonate ion saturation (ΔCO_3^{2-}; Figure A2.3; Dekens et al., 2002).

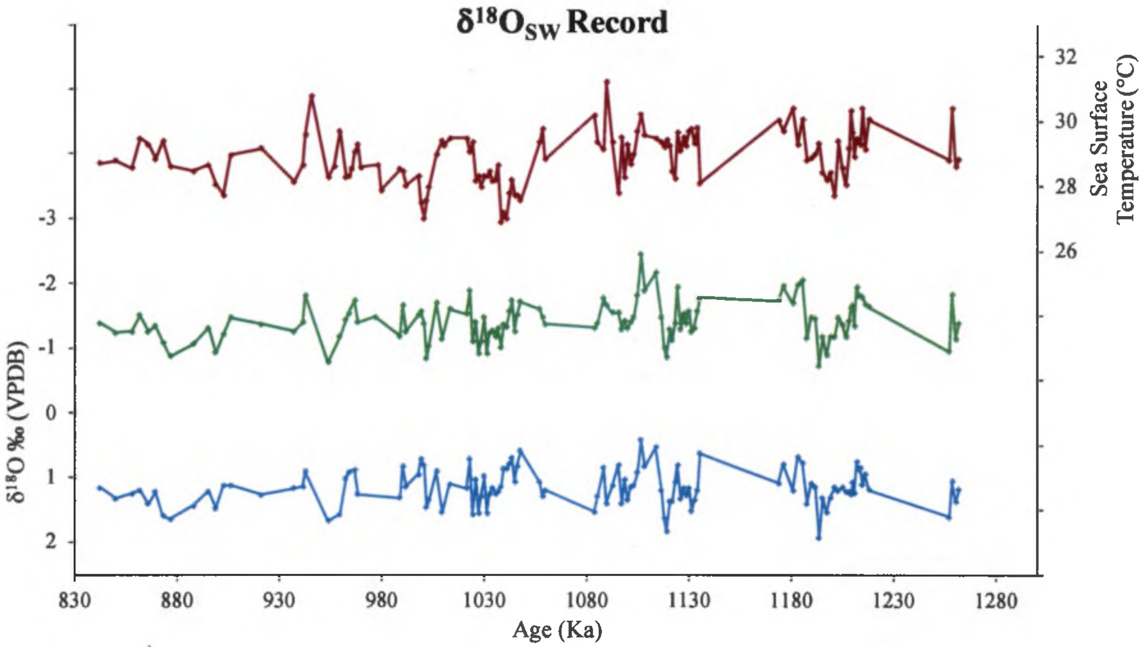

Figure 6 A figure depicting the initial *G. sacculifer* $\delta^{18}O_{CaCO3}$ data (green) and the SST record (red), which were utilized to generate the $\delta^{18}O_{SW}$ record (blue). The effect of water temperature on foraminifera shell calcification can be mathematically removed from $\delta^{18}O_{CaCO3}$ in order to approximate $\delta^{18}O_{SW}$ (Bemis et al., 1998).

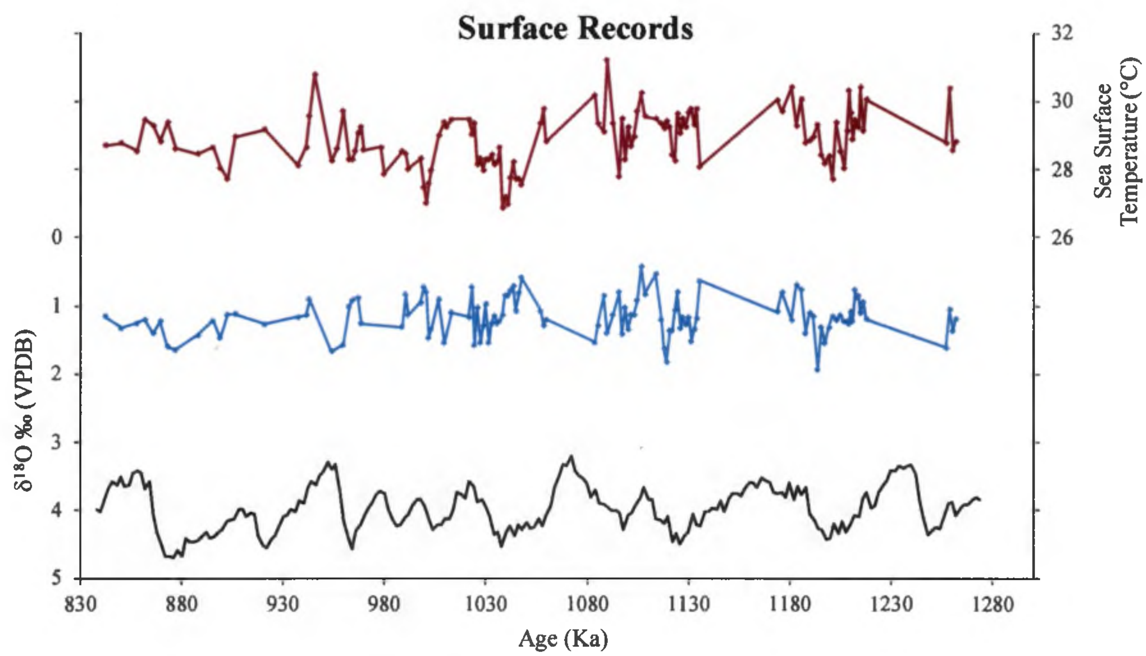

Figure 7 The final *G. sacculifer* SST (red) and $\delta^{18}O_{SW}$ (blue) results compared to the LR04 global benthic $\delta^{18}O$ stack (grey; Lisiecki & Raymo, 2005).

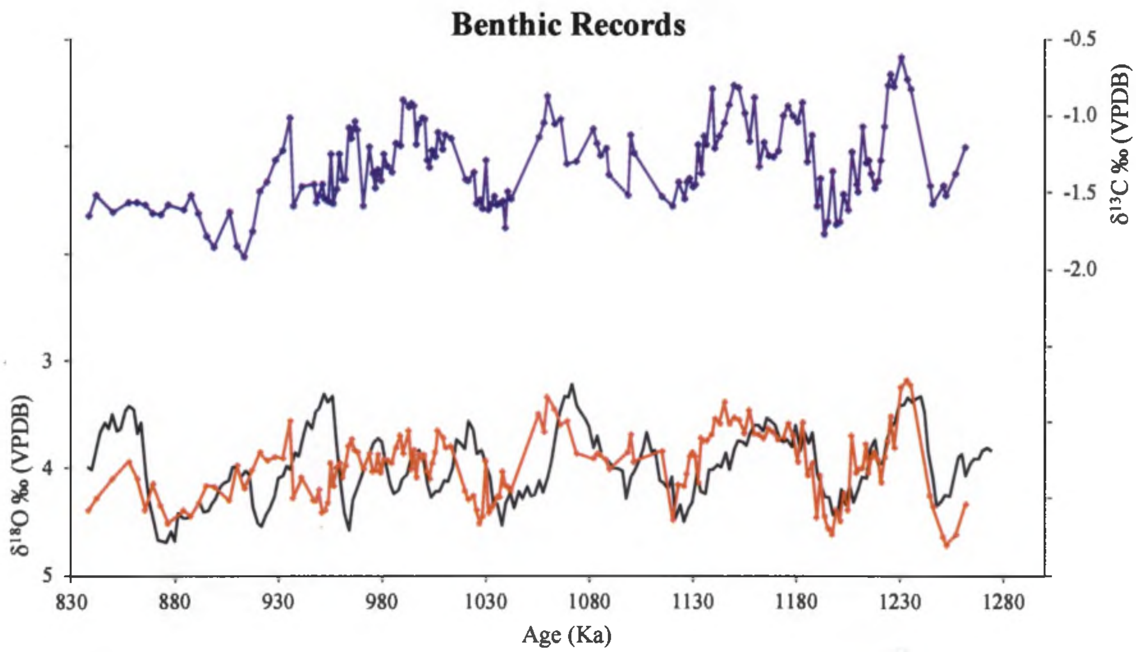

Figure 8 A comparison of the *U. peregrina* $\delta^{18}O$ (orange) and $\delta^{13}C$ (purple) records against the global LR04 benthic $\delta^{18}O$ stack (grey; Lisiecki & Raymo, 2005). The features within the site U1452 records are offset in time from the glacial-interglacial features in the LR04 $\delta^{18}O$ stack.

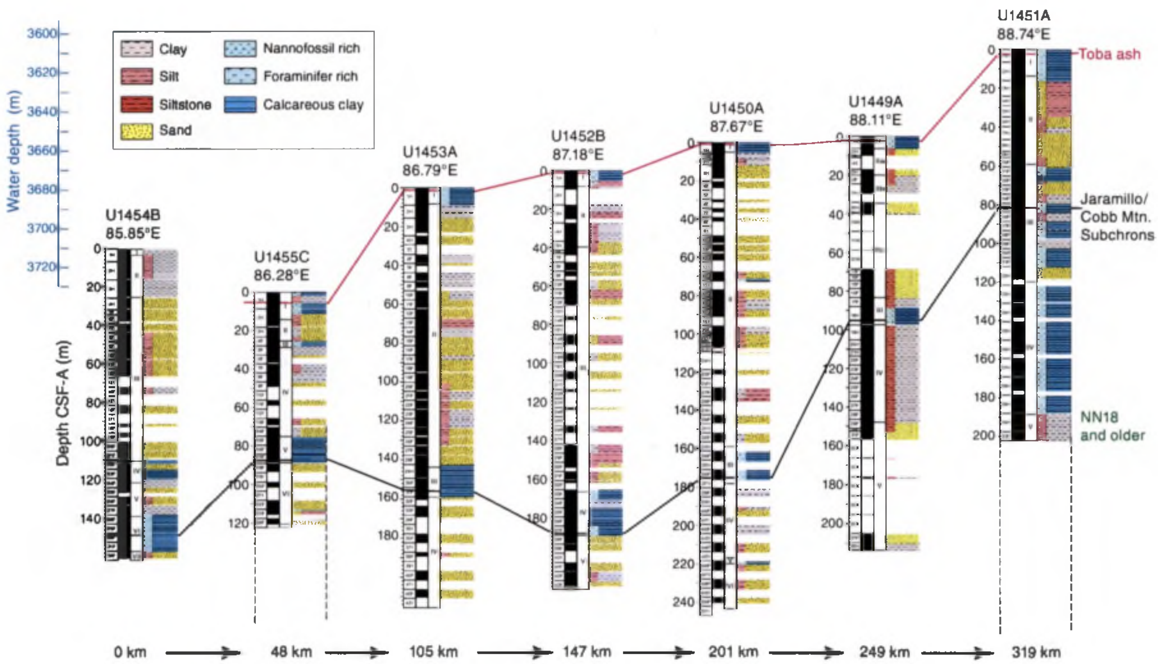

Figure A1.1 A figure from the IODP 354 Preliminary Report of stratigraphic columns from all sites within the 354 transect (France-lanord et al., 2015). site U1452, used in this study, includes a hemipelagic layer identified by the presence of the Jamarillo/Cobb Mtn. magnetic subchrons that begins at ~184 CSF-A. The Jamarillo/Cobb Mtn. subchrons can be observed at all seven 354 sites, at varying depths and thicknesses. A black line demonstrates this by connecting the location of the subchrons within each sites' stratigraphic columns.

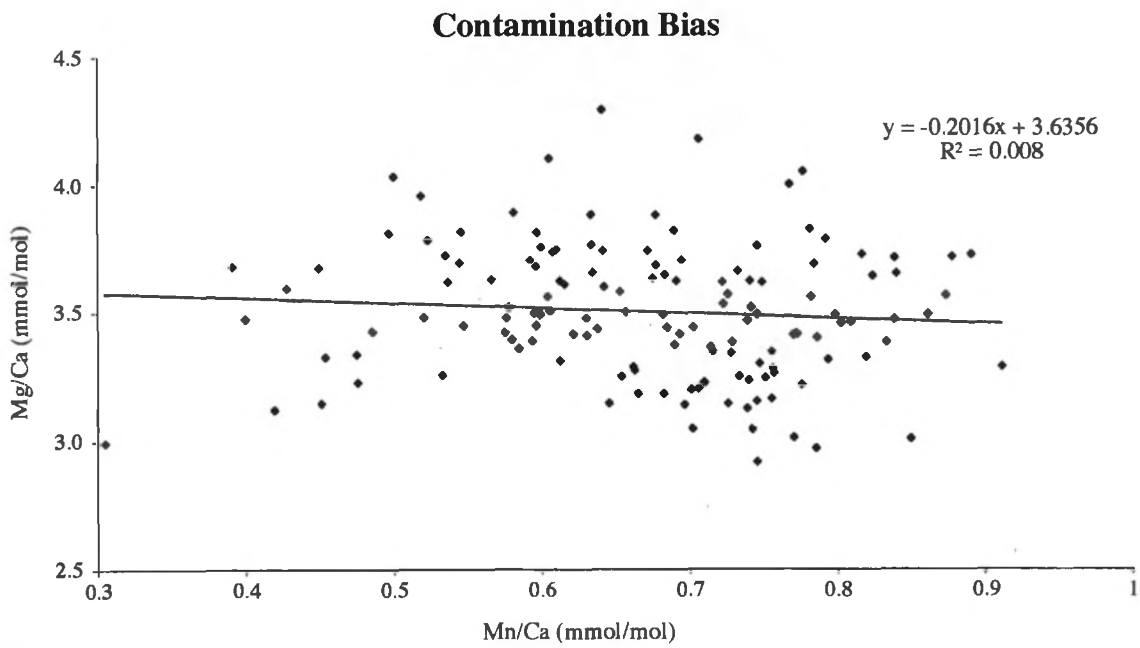

Figure A2.1 A scatterplot to observe correlation between *G. sacculifer* Mn/Ca, an indicator of contamination or insufficient cleaning, and Mg/Ca. A correlation between the variables, indicated by trendline slope or high R^2 value, would suggest potential contamination.

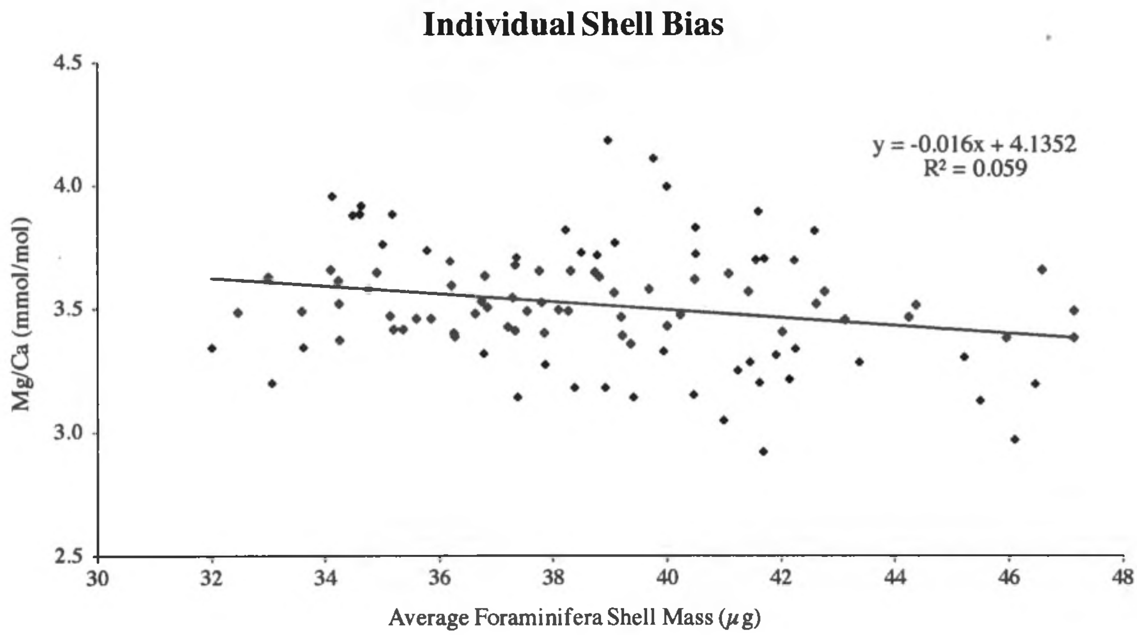

Figure A2.2 A scatterplot to observe correlation between the average *G. sacculifer* shell mass and Mg/Ca. A correlation between the variables, indicated by trendline slope or high R^2 value, would suggest the bulk samples are being biased by individual shell characteristics. This would be the result of poor homogenization of shell fragments before division into aliquots for cleaning & analysis.

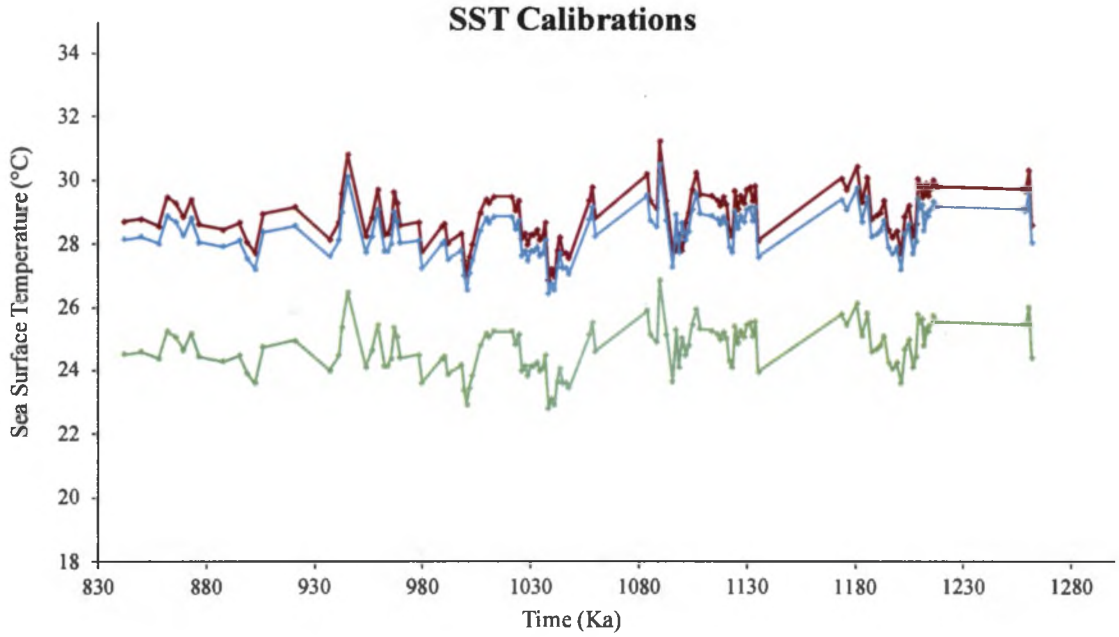

Figure A2.3 A comparison of a general SST calibration equation (light green; Anand et al., 2003) and two dissolution-corrected calibrations (Dekens et al., 2002) used to generate the Site 1452 SST record. Since site U1452 located at ~3670m water depth and subject to the effects of dissolution, the two dissolution calibrations, water-depth (blue) and carbonate ion (ΔCO_3^{2-}; red), are more appropriate methods to calculate SST. The two dissolution calibrations resulted in very similar SST records, but the water-depth equation is specific/ to either the Pacific or Atlantic basins and site U1452 is located in the Indian Ocean. Therefore, the ΔCO_3^{2-} calibration was chosen for the site U1452 SST record.